The effect of tooling design and properties of materials on fracture and deformation through equal channel angular pressing technique

Nagendra Singh[1*] and *Manoj* Kumar Agrawal[1]

[1]Department of Mechanical Engineering, GLA University, Mathura, UP, India-281406
[2]Department of Mechanical Engineering, Institute of Engineering and Technology, Khandari Campus, Agra, UP, India-282002

Abstract. The submicrometer range of grain sizes was reached for AA5083 by using equal channel angular pressing at room temperature. While the submicrometer grains of AA5083 were stable up to annealing temperatures of 300 °C, the stability of these grains was only moderately maintained up to annealing temperatures of about 200 °C. Tensile tests conducted after one pass of equal channel angular pressing—that is, strain introduction of roughly one—showed a significant increase in the 0.2% proof stress and ultimate tensile stress values for each alloy. Concurrent with this improvement, the elongations to failure decreased. The analysis shows that the square root of the magnesium content in each alloy corresponds with the magnitudes of these stresses. In samples that were cold rolled, comparable values of proof stresses and ultimate tensile stress were obtained at equivalent strains. However, because of the induction of a very small grain size, elongations to failure were higher after applying equal channel angular pressing to similar strains greater than one. The effects of material constitutive behaviour, tool design, and friction conditions on metal flow, stress fields, and the tendency for tensile fracture during the equal channel angular pressing process were studied using a finite element modelling technique. A degree of non-uniform flow was noted that extended past the head and tail of the extrusion when materials were subjected to equal channel angular pressing with varying constitutive behaviours or when utilising tooling with a radiused front leg. It is anticipated that tool design and material qualities will have a considerable effect on tensile stresses and, in turn, the development of tensile damage during equal channel angular pressing.

1 Introduction

The current study aimed to fill this gap by focusing on two main objectives. Firstly, it aimed to determine if significant improvements in the sizes of grain commercially available Al alloys could be achieved using the ECAP procedure at room temperature. Secondly, it sought to analyze the tensile properties of these materials after being pressed and determine the

* Corresponding Author: singh.mech2008@gmail.com

thermal stability of any ultrafine grain formations. ECAP has gained significant interest as a metal-working technique for inducing substantial plastic stresses and the development of extremely thin metal microstructures [8]. This process involves subjecting the material to shear deformation as it traverses the junction of two equal-sectional-area channels, meeting at a specific angle 2ϕ. The advantage of ECAP lies in its ability to impose significant strains without altering the cross section of the metal, making it particularly beneficial for metals that tend to exhibit segregation issues whenever huge ingots are cast. These analyses involved approximations of slip-line fields to estimate the necessary loads for achieving shear strain in frictionless ECAP, taking into account the die geometry. Follow-up measurements using visioplasticity or plasticene techniques were conducted to assess the shear strain in one pass and more than one pass pressings [9]. The results demonstrated that the deformations experienced in the central regions of the billets away from the die walls, aligned well with the predicted values. The formation of nonuniform deformations observed in the ECAP of aluminum, using a die configuration similar to the one employed in the study, was consistent with the findings obtained from finite element method analysis. The use of ECAP tooling with a sliding bottom floor, a design element created especially for this purpose, could reduce the presence of deformation non-uniformities. It is reasonable to expect that they can significantly affect the likelihood of fracture occurrence during the ECAP process, particularly when working with challenging materials. To validate the significant findings obtained from finite element modeling, observations from ECAP experiments conducted. The fabrication of materials with sizes of ultrafine grain has been significant attention due to their desirable properties. The materials fabricated using these methods tend to have incomplete density, which limits their overall quality [10]. Additionally, scaling up these techniques to produce large bulk samples presents significant challenges. Consequently, researchers have turned their attention towards alternative approaches that involve severe plastic deformation to develop ultrafine-grained materials. There are currently two main methods for applying a sample to an extremely intense plastic strain. The first method known as ECAP entails pushing a piece through a die while preserving the sample's original cross-sectional dimensions in order to generate a significant strain. The second method, referred to as torsion straining, involves applying a torsional force while under intense pressure in order to significantly total strain a disc. Both ECAP and torsion straining procedures offer the potential to generate products with very fine grain sizes in the submicrometer or nanometer scale. However, one drawback of torsion straining is that it is limited by the size of the specimens, as the discs typically have diameters of around 10-15 mm.

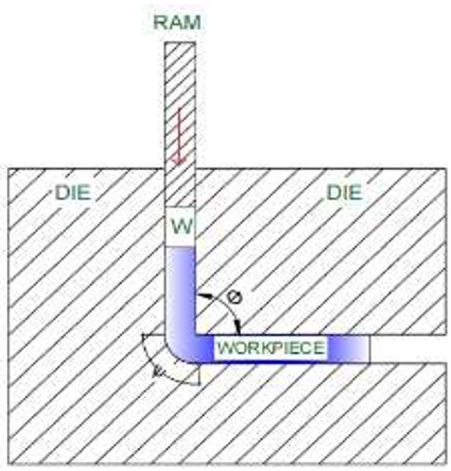

Fig. 1. The schematic sketch of ECAP process [6].

Consequently, while torsion-strained samples may display unique properties, scaling up the procedure for large bulk material fabrication remains challenging. As a result, the attention and emphasis have shifted towards the development and assessment of the ECAP procedure, which offers promising possibilities for producing and evaluating ultrafine-grained materials on a larger scale [11]. ECAP is a SPD technique used to refine the grain structure and increase the mechanical properties of metals. It involves pressing a metal billet or specimen through a die with intersecting channels. The most common die geometry used in ECAP is also known as the Conform Process or the Bridgman Process. The X-plane represents the horizontal plane of the facility. It is the plane in which the ECAP die is mounted and secured. The x-plane is parallel to the die face and contrary to the direction that the billet is moving. The y-plane represents the vertical plane in the ECAP facility. It establishes the direction of the billet movement and is perpendicular to the x-plane [15]. The billet is typically placed in a holder or a ram that applies pressure to push the billet through the channels of the die. The movement in the Y-plane allows the billet to undergo plastic deformation as it passes through the channels. The z-plane represents the depth or thickness dimension of the ECAP facility. It is perpendicular to both the x-plane and the y-plane. The z-plane determines the length of the channels in the Equal Channel Angular Pressing die, which defines the amount of material that can be processed during each pressing cycle. In ECAP, there are four fundamental pressing routes that describe the different ways the billet can be oriented and rotated during the deformation process. In Route A, the billet is loaded into the ECAP die in a specific orientation, and no rotation of the billet occurs during deformation. The billet is pushed through the die without any change in its orientation [17].

2 Experimental Material and Procedure

2.1 Experimental Material

The material used in this study is the commercial AA5083 pressed and its chemical composition shown in table 1. The pressed is processed into a round bar specimen with a diameter of 10 mm and a length of 50 mm, and grain samples were obtained in the size of 210 μm by annealing the round bar specimen under 733K for 1.2 h. Through the die having the channel angle (ϕ) of 90^0 and the corner angle (ψ) of 20^0 at the temperature of 483K with the strain rate of 2.2 mm/s, the specimen was processed with one to eight passes via route B_C where the sample is rotated by 90^0 in the same sense between each pressing. To minimize the friction with the die, MoS_2 lubricant was applied to the specimen surface. The schematic illustration of the ECAP pressing die is shown in Fig. 2.

Table 1. Aluminium alloy 5083 chemical composition [7]

Element	Si	Fe	Cu	Mn	Mg	Zn	Ti	Cr	Al
%	0.4	0.4	0.1	0.4-	4.0-4.9	0.25	0.15	0.05-0.25	Balance

2.2 Experimental Procedure

This route is also referred to as the "no rotation" or "straight" route. In Route B_A , the billet is loaded into the ECAP die in a specific orientation similar to Route A . However, after each pass, the billet is rotated by 90^0 near its longitudinal axis before being pushed through the die again. This 90^0 rotation is carried out to prevent excessive deformation along a single shear plane. Route B_A is often called the "90^0 rotation" or "simple shear" route. In Route B_C, the billet is loaded into the ECAP die with an initial rotation of 90^0 around its transverse axis.

After each pass, the billet is further rotated by 90^0 around the same axis before being pushed through the die again. This rotation helps distribute the strain and avoid preferential deformation along specific planes. Route B_C is known as the "90^0 rotation" or "double shear" route. In Route C, the billet is loaded into the ECAP die with an initial rotation of 180^0 around its transverse axis [18]

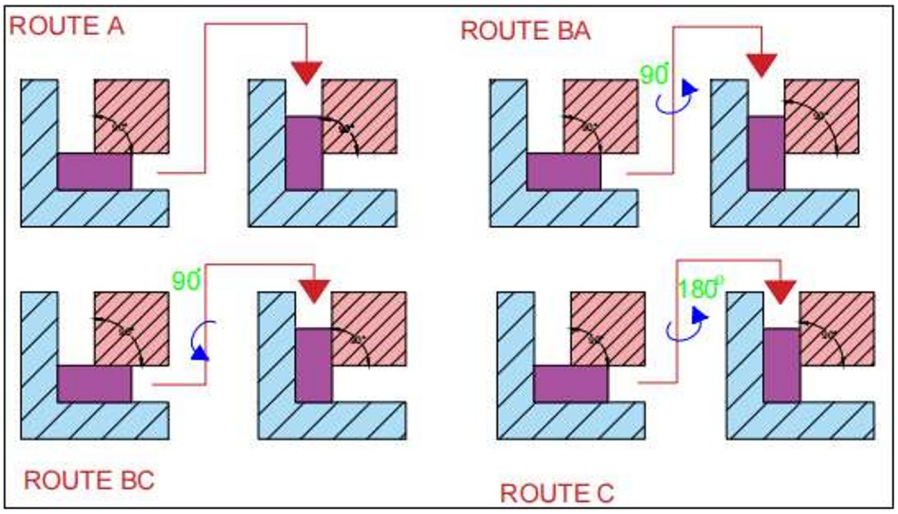

Fig. 2. Schematic diagram of different processing routes in Equal Channel Angular Pressing [19].

After each pass, the billet is rotated around by 180^0 near the same axis before being pushed through the die again. The 180^0 initial rotation in this route enables a more uniform strain distribution. Route C is often referred to as the "180^0 rotation" or "multi-axial" route. These four processing routes in ECAP allow for different strain distributions and deformation characteristics, leading to variations in the resulting mechanical properties and microstructure of the processed material. The choice of the processing route depends on the desired microstructural modifications and the mechanical properties targeted for improvement in a specific application. To attain substantial total strains, repeated pressings can be carried out in ECAP, therefore the sample's cross-sectional dimensions are unaffected. By rotating the sample between consecutive pressings, it becomes possible to induce different microstructures in a chosen material. During the passage of the sample across the shearing plane, this rotation modifies the shearing plane and shearing direction. While it is possible to manually rotate samples between successive pressings in laboratory experiments for study, the practical application of ECAP in industrial settings requires the development of a multi-pass facility. Such a facility enables the accumulation of large total strains in a one pass by die. The scientific community has shown significant interest in due to their distinct mechanical and physical characteristics of ultrafine-grained materials [20]. Producing such materials in bulk is economically profitable. The deformation of the material during ECAP is influenced by various factors, includes temperature, mould geometry, friction in billet & mould and plungers design. Basic mould design parameters were mainly investigated in the early investigations, such as the corner angle (ψ) and channel angle (ϕ) between the two mould channels. The estimated plastic strain value (ε) represents an average value $\phi = 90^0, \Delta\varepsilon = 1.155$ and does not fully explain the actual behaviour of deformation, which is influences from friction, mould geometry, material characteristics, and other relevant parameters. In order to gain insights into the behavior of materials undergoing ECAP, computer simulation techniques have been extensively employed in various research studies [21]. These simulations, utilizing both finite element analysis and experimental

investigations, have enabled the examination of billet deformation under different ECAP conditions. The formation of die gap corners influenced by the rate of material strain hardening and the effect of mold geometry on the ECAP process. The FEM serves as an efficient tool for predicting behavior of material and designing ECAP molds. Changing channel moulds that help prevent tensile stressing modes can be designed using finite element simulations. While studies on the ECAP technique and behavior of materials are important, a quality standard for the ECAPed billet must be established as well., as this criterion forms the basis for practical applications [22]. The microstructure of the billet is significantly influenced by the shape of the mould corner and further advancements in ECAP technology can be achieved by considering effect of back pressing plungers. To assess the quality control of billets produced through ECAP, an index was introduced, taking into account the findings from computer simulations. These analyses aimed to determine the optimal working condition for achieving high-quality ECAPed billets. SPD is a highly efficient method for manufacturing bulk metals with ultrafine-grained structures at the submicron or nano-scale. The focus of the current study was on predicting the deformation behavior of AA5083 and analyzing its flow characteristics under different channel angles, while taking into account various hydrostatic pressure situations [23]. Numerous FEM studies have been provided to investigate the material deformation behaviour, specifically focusing on the influence of angle of channel 90^0 and $120^0$and outer corner under frictionless conditions. It has been observed that when subjected to one-pass ECAP, the billet exhibits non-uniform deformation on its surface with or without fillets. However, the introduction of fillets at the corner angles improves deformation homogeneity $\phi < 90^0$and $\phi > 90^0$, as evidenced by both simulation and experimental results. The deformity behavior becomes more complex when using acute channel angles, leading to a lack of smooth flow and causing strain heterogeneity. On the other hand, obtuse channel angles result in a smoother deformation behavior. With acute channel angles, the limited freedom of sample flow leads to strain heterogeneity. Conversely, strain heterogeneity arises with obtuse channel angles due to the formation of large corner gaps and inadequate plastic zone length. The deformed geometry for strain hardening materials is expected to be essentially unaffected by the angle of die corner. The analysis focused on the use of annealed pure copper as the workpiece material, and the results indicate that there are numerous opportunities to manipulate the materials bending behaviour during ECAP by merge different die and workpiece geometries [24].

3 Experimental Results

3.1 Deformation Analysis Technique with Effect of Friction

In the depicted region, R_1 significant shear deformation is observed, while in another region, denoted as the "zone," no grid distortion $R_2$is evident. The difference in shear deformation between these two zones R_3 and R_4 is attributed primarily to the friction between the mould wall and the billet. For Route C , the onset of shear deformation occurs at $R_5$the "zone" and concludes at the "zone." Notably, a distinct and intense deformation is observed at the "zone," which originates from the left and bottom corner of the billet during the early stages of the ECAP process [71]. Figure 14 provides a visual representation of the grid deformity for every pass. Due to the low strain gradient in the nearby deformation field and the comparatively modest plastic deformation of the square grid (strain value of 0.5), there is little driving force for grid distortion. The grid is severely constrained, leading to a plastic deformation amount of 1.4, by the inner corner of the mould and the strong strain gradient of the neighbouring deformation field. The specimen's axial centre is where the grid is located, and its plastic strain following ECAP is 1.0. The strain values obtained using Equation 1 are calculated to

be 1.155, demonstrating good agreement with the measurements in the region C_1near the intersection point between Route C and the line L_4. However, noticeable differences in strain values are observed in the regions T_4 and B_4. Controlling the billet's microstructure is mostly dependent on the plastic deformation of metallic components during the mould passage. The actual pattern of material flow solely through measurements can be challenging [72]. When a mould corner is encountered during the ECAP process, the use of computer simulations gives the chance to predict the material flow behaviour. The DEFORM software was employed for simulating the equal channel angular pressing process. The plastic strains obtained from the finite element analysis (FEM) show values ranging from 0.5 to 1.4. When comparing these results with measurements and calculations based on equations, along with simulations using DEFORM, it can be concluded that the simulation reasonably predicts the material's response during the ECAP process. Consequently, the outcomes of computer simulations offer a viable means of explaining various ECAP conditions without the necessity of conducting actual experimental tests [73]. Figure 14 display the deformation behaviors of billets that have undergone partial deformation with and without friction respectively for a angle of mould 90^0. Its important to make it clear that the grids shown in the figures do not represent the actual finite element mesh. Which originates from the lower part of the mold, limits the material's movement at this outer corner. Ultimately leading to the detachment of the fragment from the billet [74]. The fragment left at the corner after the passage is extremely hard and has the potential to alter the original shape of the mold corner. Consequently, it is necessary to remove the fragment in order to restore the desired sharp corner. A Comparing the plastic strain differential between the top and bottom components reveals that the top part deforms more quickly, while the bottom part requires a longer duration. The presence of friction serves as a back pressure, causing the onset of plastic deformity to occur earlier in the case with friction compared to the case without friction [75]. Two scenarios including one with and one without friction are used to explain how the sample deforms. In the case with friction, plastic deformation occurred earlier compared to the case without friction. In the absence of friction, the highest plastic strain noted at the upper section of the billet was 1.14. However, in scenarios involving friction, this value decreased to 1.08. Friction's existence impeded the material's movement at the surface area, resulting in decreased deformation within the billet's inner portion [76]. The presence of friction imposed a constraint on the flow of material, particularly at the bottom part of the specimen. This constraint led to a decrease in material deformation at the bottom compared to the top, resulting in a reduction in the strain differences between the two regions from $\Delta\varepsilon = 0.62$ to $\Delta\varepsilon = 0.60$. Additionally, the stress histories of the top part differed between the cases with and without friction. Specifically, prior to the corner passage, the top part experienced a most extreme compressive stress T_1. However, as the corner was traversed, this compressive stress transformed into high tensile stress. During this stage, there is a high likelihood of crack formation at the top part of the specimen. While the top part experiences extreme stretching, the corresponding center and bottom parts do not undergo shear deformation line L_2. The difference in peak tensile stress at the top part between the cases with and without friction ΔPis 5 MPa [77]. For practical applications of cold working with pure aluminum, the friction effect is not considered critical, especially with a friction coefficient of friction ~0.2. The risk of cracking is not always higher when friction is higher [78]. This is because at higher temperatures, the ductility of the material also increases, reducing the resistance to material flow and facilitating the ECAP process.

3.2 Flow Rate and Shape of Back Pressing Plunger

Figure 14 illustrates the deformation characteristics of the 5083 alloy. Notable differences in rotation are observed at the leading edge of the billet. In contrast to the 5083 alloy, pure

aluminum demonstrated higher rotation at this front section. The 5083 alloy presented a more consistent and evenly spread material flow. It's also important to highlight that the horizontal distances from the corners are 5 mm for pure aluminum and 3 mm for the 5083 alloy. This variation in consistency can be attributed to the unique stress and strain responses exhibited by the materials. The 5083 alloy, characterized as a solid solution hardened material, displays this difference [79]. Consequently, it was observed that the 5083 alloy's strain hardening rate remained lower than that of pure aluminum during the ECAP process. It's crucial to mention that the analysis was carried out with the assumption of no friction, which in turn prevented any separation of the fragment at the outer corner. Upon comparing the variations in accumulated plastic strain between the upper and lower sections in both range and peak values, it became evident that the 5083 alloy showed lesser disparities in plastic strain in contrast to pure aluminum. Pure aluminum indicated greater deformation at its upper part and less deformation at its lower part when compared to the 5083 alloy. Additionally, owing to its initially strengthened state, the 5083 alloy displayed a quicker approach towards reaching the ultimate deformation state. Two materials were also subjected to a comparison. Interestingly, right before traversing the corner, both materials demonstrated the highest compressive stress at the upper segment. However, what stands out is that the magnitude of this peak compressive stress was roughly two times greater for the 5083 alloy compared to pure aluminum. It's worth highlighting this fact, especially when considering that the yield strength of the 5083 alloy is five times higher than that of pure aluminum [80]. It becomes evident that the process of material deformation during ECAP is influenced not solely by the yield strength but also by the material's stress and strain response. While transitioning around the corner, the compressive stress within the 5083 alloy experienced a sudden shift towards high tensile stress. Despite the fact that the maximum principal stress surpassed the yield stress, it remained beneath the material's tensile strength. Given the outcomes of this stress analysis, it is implied that cracks might not form in the material that has undergone ECAP. A substantial rise of about 42% in principal stress is projected to be necessary to induce fracture in the upper portion of the specimen. The strain of the cell measured at position along route B was 0.4, which is greater than the fracture strain [81]. However, no cracks were observed in the ECAPed specimen. This shows that hydrostatic compressive pressure was used to create the actual deformation during the ECAP procedure. To fabricate fine-grained material from the 5083 alloy using ECAP, three times higher power is required compared to pure aluminum. The application of higher power results in increased stress on the ECAP mold, which imposes limitations on the materials suitable for equal channel angular pressing processing. Introduction of friction during the ECAP procedure led to a reduction in the corner distance in figure 15, thereby facilitating a more even distribution of plastic deformation. The aim of achieving well-defined corners with complete corner filling leads to a uniform plastic deformation pattern, aligning with the desired outcome of the ECAP process. Utilizing a back pressing plunger can fulfill a role akin to friction by assisting in the thorough filling of mold corners [82]. A comparison is drawn between deformations occurring under back-pressure conditions employing plungers featuring flat and tapered surfaces. It becomes feasible to attain plastic strain values surpassing unity across the entire billet section. To improve efficiency, the implementation of a tapered back pressing plunger was introduced to tackle this concern and guarantee comprehensive plastic flow [83].

4 Experimental Discussions

4.1 Microstructure and Tensile Properties of Specimem

Figure 15 displays typical microstructures of commercial alloys in their as-pressed condition, with chosen area electron diffraction patterns gathered from various areas inside these microstructures. For each sample the number of ECAP passes is given. It can be seen that the AA5083 alloy has the highest average grain size [84]. This confirms that room temperature ECAP is highly effective in achieving significant refinement of grain in AA5083. The SAED patterns also indicate that there are boundaries with significant misorientation angles separating the grains in these materials [85]. A common feature seen in these microstructures is the existence of a high density of dislocations within the grains, along with numerous grain boundaries that have a wavy or unclear appearance. Comparable findings of unclear boundaries have been documented in different materials that have undergone severe plastic deformation to attain ultrafine grain sizes. These characteristics are often understood as signs of boundary configurations with high energy and a lack of equilibrium.

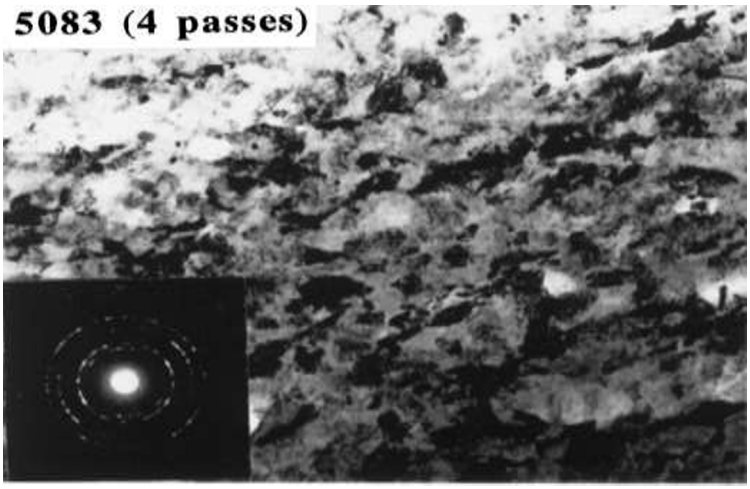

Fig. 3. Typical microstructures after ECAP 5083 alloy after four passes [86].

The quantity of passes through the die correlates directly with the equivalent strain, and data points at an equivalent strain of zero represent the examination of samples in their annealed state, without undergoing any Equal Channel Angular Pressing. It can be noted that both the 0.2 percent proof stress and ultimate tensile strength show a rapid rise following a single pass through the die, whereas subsequent increments become more gradual. Furthermore, it is clear that the AA5083 alloy displays the greatest 0.2 percent proof stress and UTS following a sole pass through the die, aligning with an equivalent strain of 1. Its crucial to highlight that there is no substantial additional decrease in strength with further pressings. Instead, the elongation until failure maintains a relatively steady value at higher equivalent strains, and in certain instances, it might even slightly rise for the AA5083 alloy [87]. The recorded fluctuations in strength and ductility mentioned in Figure 15, suggest the possibility of leveraging ECAP to enhance the resilience of a material. Figure 16 depicts the correlation between the 0.2 percent proof stress, ultimate tensile strength and elongation at failure concerning the equivalent strain during ECAP procedures. It is evident that the 0.2 percent proof stress and UTS display analogous changes as the equivalent strain increases. The extension to failure is lower for the samples that underwent cold rolling, especially at an equivalent strain close to 3. Unfortunately, Therefore, to obtain a tensile samples with a

thickness of 2 mm, an nearest billet thickness of ~65 mm is required to achieve an equivalent strain of 4 in the ECAP process [88]. The enhanced ductility that can be achieved through ECAP compared to cold rolling.

4.2 Thermal Stability of The Ultrafine Grains For Aa5083

These microstructures were obtained after subjecting the alloys to equal channel angular pressing followed by subsequent static annealing at three different temperatures: 100 0C, 200 0C, and 300 0C. The microstructures are accompanied by corresponding SAED patterns. It is observed that the microstructures after annealing at 100 0C are similar to those obtained after ECAP. The selected area electron diffraction (SAED) patterns also verify the existence of high-angle boundaries [89]. Heat treatment at 200 0C leads to a decrease in the density of dislocations within the grains, and the grain boundaries become more distinct. Nevertheless, there is minimal to no enlargement of the grain size and it remains within the submicrometer range.

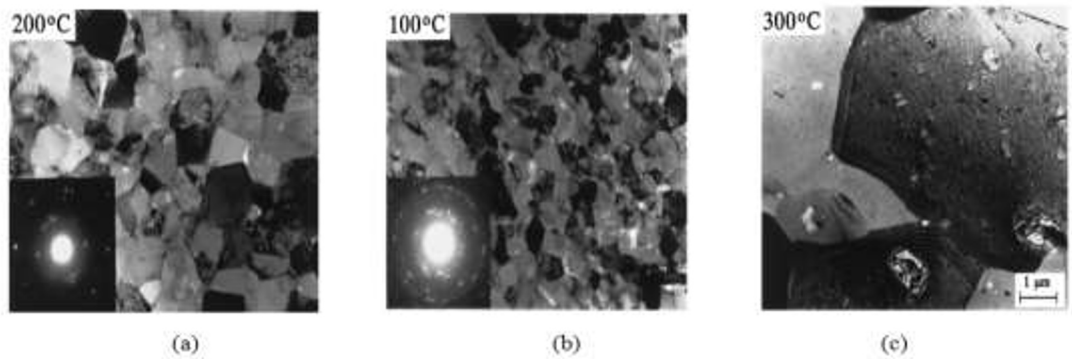

Fig. 4. Microstructure of the AA5083 after ECAP at temperature (a) 200 0C (b) 100 0C and (c) 300 0C [90].

To determine how annealing treatments following ECAP affect the tensile characteristics, specimens of AA5083 tensile strength were cut after six and eight pressings. Before being put through a tension test, these specimens were annealed for one hour at temperatures as high as 300 0C. The stress-strain curves for different conditions were obtained, including samples that were annealed before ECAP and samples that underwent ECAP without subsequent annealing. There are two different types of behaviour visible in the stress-strain curves. For samples with extremely small grain sizes, such as the as-ECAP sample and the specimens that underwent ECAP before being annealed at 200 °C. As the strain increases, the flow stress initially rises to a maximum and then progressively falls [91]. The characteristic of strain-hardening metals, where the material becomes stronger as it is deformed. The annealed samples before and after ECAP, as well as those annealed at 300 0C. The grain sizes are not submicrometer anymore. The stress-strain curves exhibit a protracted strain hardening period, indicating that the material continues to strengthen as it is deformed. This analysis of the stress-strain curves provides insights into the different mechanical behaviors exhibited by the samples under various annealing conditions after ECAP. After ECAP and subsequent annealing at 300 0C, the materials exhibit larger flow stresses compared to the unpressed condition. Because of the smaller grain sizes obtained during ECAP and annealing at high temperatures flow stress has increased. The stress-strain curves after annealing at 250 0C show intermediate behavior, indicating the onset of grain growth [92]. It should be noted that slightly higher stresses observed at compared to the "as-

ECAP" materials, may be attributed to experimental scatter rather than significant variations in the annealing temperature. It displays charts of the UTS and the 0.2 percent proof stress for these two alloys in relation to the annealing temperature. Plots for the elongation to failure that correlate. These characteristics are mostly unaffected by the annealing temperature until 200 0C. However, once the temperature surpasses 200 0C, the 0.2% proof stress and ultimate tensile strength (UTS) decline, while the elongation at failure rises. This suggests that annealing at higher temperatures leads to a decrease in strength and an increase in ductility [93].

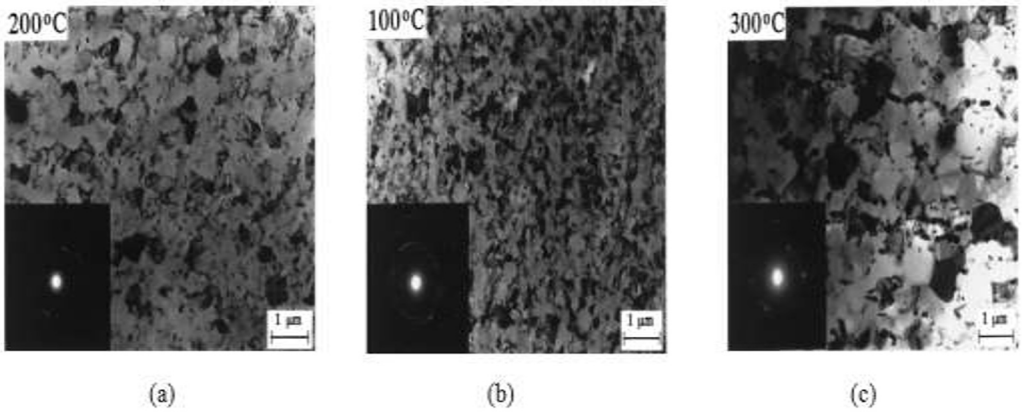

Fig. 5. The microstructure of the 5083 alloy following six ECAP passes and subsequent 1-hour annealing at different temperatures (a) at 200 0C (b) at 100 0C and (c) at 300 0C [94].

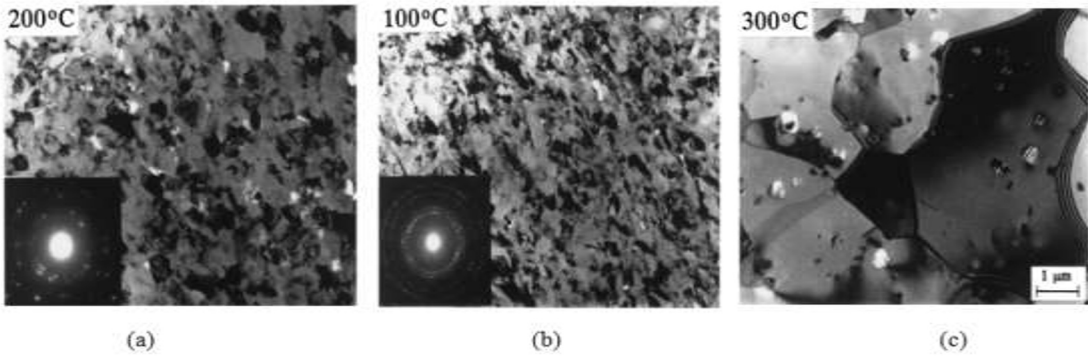

Fig. 6. Microstructure of the 5083 alloy after eight runs of ECAP and 1 hour of annealing at (a) 200 0C (b) 100 0C and (a) 300 0C [95].

In order to evaluate the validity of the Hall-Petch relationship within these alloys, the experimental results were graphed by establishing a connection between the 0.2% proof stress and the reciprocal square root of the determined grain size for each annealing condition. Despite the variation in grain sizes observed between the two alloys, all data points for both alloys closely adhere to a single linear trend on the graph. This graphical representation validates that the application of ECAP followed by annealing aligns with the predictions established by the Hall-Petch relationship [96].

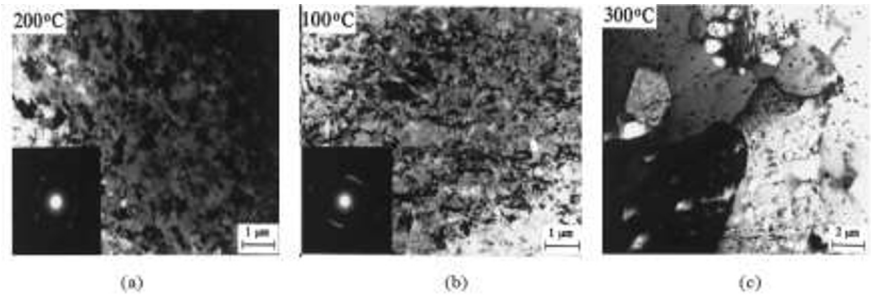

Fig. 7. Microstructure of the 5083 alloy after ECAP through six passes and annealing for 1 h at temperatures of (a) 200 0C (b) 100 0C and (c) 300 0C [97].

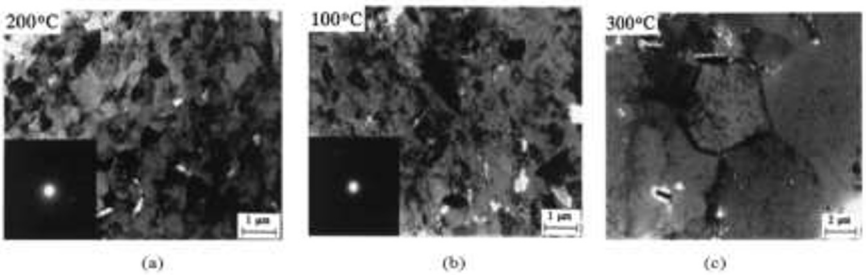

Fig. 8. Microstructure of the 5083 alloy after ECAP through four passes and annealing for 1 h at temperatures of (a) 200 0C (b) 100 0C and (c) 300 0C [98].

4.3 ECAP Process at Room Temperature

To obtained results in this investigation provide compelling evidence that room temperature ECAP is highly effective in achieving significant grain refinement in AA5083 alloy. Even after undergoing a relatively limited number of passes through the die, the alloys achieve grain sizes within the submicrometer range as a result of the ECAP process. This decrease in grain size is coupled with a proportional rise in both the 0.2% proof stress and the ultimate tensile strength, while the elongation at failure experiences a decline. The enduring nature of these ultrafine grains is proven through static annealing, where they retain a considerable level of stability in each alloy even when subjected to temperatures up to 200 0C. In the case of AA5083, the grains retain their submicrometer size even at annealing temperatures of at least 300 0C [99]. Experimental findings on the alloys demonstrate a strong correlation with the Hall-Petch relationship over a range of grain sizes spanning approximately 0.25 to 30 μm.

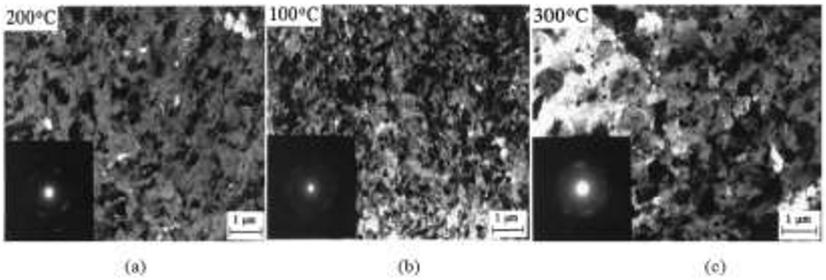

Fig. 9. Microstructure of the 5083 alloy after ECAP through four passes and annealing for 1 h at temperatures of (a) 200 0C (b) 100 0C and (c) 300 0C [100].

The results show that the existence of flaws, which alter the mobility of dislocations has an impact on the values of the 0.2% proof stress and the UTS. The square root of the concentration of the pertinent defect has a linear connection with the stress level. This relationship is illustrated in Figure 21, where the square root of the aluminium concentration in atomic percent $(C_{MG})^{\frac{1}{2}}$ is displayed against the 0.2% proof stress and the UTS. In the case of AA5083, the data points appear slightly below the line in Figure 22 [101].

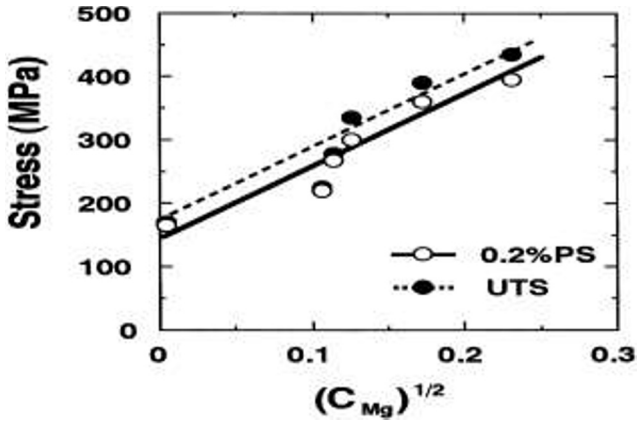

Fig. 9. Variation of the ultimate tensile strength and the 0.2% proof stress for AA5083 with respect to the square root of the aluminium content. [102].

This study presents a comprehensive comparison between ECAP and cold rolling, specifically focusing on their effects on the mechanical properties. The experiments conducted on the 5083 alloy reveal that, when considering equivalent strains, the 0.2% proof stress and the ultimate tensile strength values are altered similarly by ECAP. However, elongation to failure of ECAP is higher at equivalent strains than 1. This increased ductility can be due to the ECAP induced reduction in particle size. Future investigations should concentrate on evaluating the disparities in texture that arise from these distinct processing methods [103].

4.4 Deformation Patterns During ECAP

Finite element method simulations were utilized to gain a comprehensive understanding of metal flow during ECAP, particularly focusing on the affecting of geometry of die. Figure 22 [104] illustrates how die geometry influences grid distortion. Nevertheless, specific differences were observed depending on the die design and the friction conditions of the slider. This was evident in simulations conducted with both the simple die and the complex die, particularly when low slider friction conditions were taken into account. The detachment of the billet from the die at the start of the pressing process, along with insufficient material filling in the lower left corner of the die. These outcomes were absent in the simulation involving the complex die when employing high slider friction conditions. These results underscore the notable impact of both die geometry and slider friction conditions on the metals flow characteristics during the ECAP procedure. The FEM grid distortion findings for tooling with a channel width of of $R_f = 0$ mm and a strain-hardening material with a value of 0.02 shown in Figure 22. exhibit several notable differences compared to the previous predictions in Figure 23. In line with the behaviour shown in the high slider friction scenario for a strain-hardening material with n equal to 1 or a m value of 0.02 the billet form was projected to retain a more square-cornered shape [105]. These variations in the FEM grid disturbance results highlight how the behaviour of the material during ECAP is sensitive to

several material factors, including the strain hardening exponent (n) and coefficient (m), as well as the impact of die geometry and slider-friction conditions [106].

The observed trends in the FEM simulations can be attributed to the influence of the strain-hardening exponent $m = 0.15$ or 0.02 on the deformity procedure occurring in the ECAP shear region. A more localised form of shear flow results when is low value $m = 0.02$ because it prevents the propagation of deformation away from the shear zone. The inclusion of strain hardening and a moderate degree of strain rate hardening effectively mitigates notable instabilities in shear concentration. This is evidenced by the results of finite element method simulations shown in Figure 23. Furthermore, the findings from the FEM model suggested that modifying the radius of the front leg within the range of 0 to 8 mm does not result in any significant alteration at $m = 0.15$ to the overall metal flow pattern. This observation holds true for a material exhibiting strain-hardening characteristics [107]. These results emphasise the significance of material characteristics, such as the strain-rate sensitivity and the strain-hardening exponent. Deformation behavior during ECAP, the simulations provide valuable insights into the underlying mechanisms governing metal flow and deformation patterns in the ECAP process.

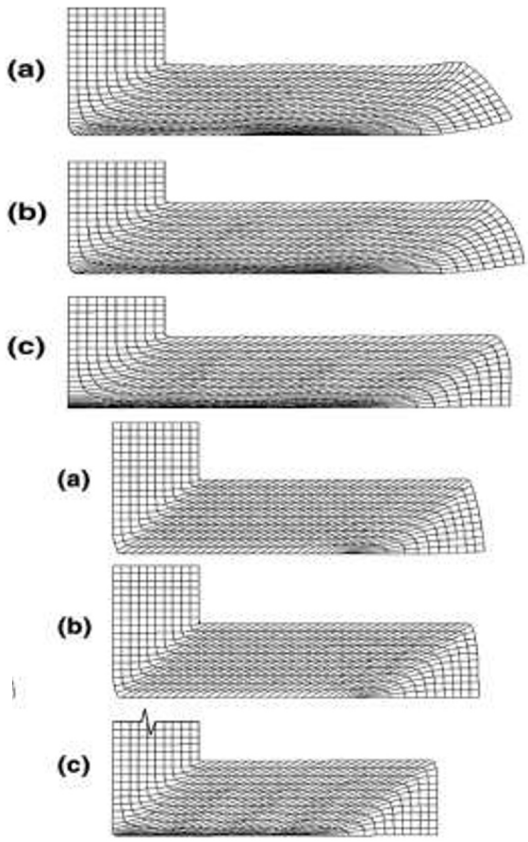

Fig. 11. Grid distortions for an ECAP of a material is strain-hardening for various passes [108].

The observed improvements in metal flow resulting from reducing the strain-hardening exponent (m) from 0.15 to 0.02 were less pronounced when utilising both the basic and sophisticated tooling with a front-leg radius of 1 mm. This highlights the important interaction between die shape and material parameters in determining flow characteristics

during ECAP. The specific combination of properties of material and geometry of die plays a crucial role in establishing the metal flow behavior during the ECAP process. While reducing the strain-hardening exponent can have a beneficial effect on metal flow, the extent of this improvement is influenced by the specific configuration of the die[109] . The intricate relationship between die geometry and material qualities, and the deformation process highlights the need for a comprehensive understanding of these factors in order to optimize the ECAP process and achieve the desired material properties. The distortions in the grid as predicted by FEM for the rigid, perfectly plastic and flow-softening material responses in both cases display analogous patterns to the behavior (both with $m = 0.15$) of the material exhibiting strain-hardening behavior $m = 0.02$. In both scenarios, the consistency of flow and the deformation characteristics at the front of the billet were primarily shaped by the type of die and the friction of the slider. Nevertheless, unlike the response observed in strain-hardening behavior, variations in the strain-hardening exponent (m) did not result in the enhancement of flow uniformity or the elimination of the more intensely sheared area at the bottom of the billet in the case of the rigid, perfectly plastic constitutive [110]. The flow characteristics and deformation behavior for these different material behaviors were primarily governed by the die geometry and slider friction, rather than the strain-hardening behavior of the material. These findings emphasize that the material behavior, including strain hardening, rigid plasticity, and flow softening, interacts with die geometry and slider friction to determine the flow uniformity and deformation patterns in the ECAP process. It highlights the complex relationship between material properties, constitutive behavior, and process parameters in influencing the metal flow during ECAP [111].

4.5 Strains and Strains Rate

This suggests that the strain distribution obtained through FEM simulations aligns with the expectations from these simplified shear models. It is important to consider these strain results in the context of the specific material behavior, die geometry, and process conditions used in the simulations. The FEM predictions provide valuable insights into the deformation patterns and can be used to analyze the distribution of strains and strain rates within the material during the ECAP process. Additional information about the materials flow behaviour is provided by the FEM predictions of effective stresses and strain rates in the deformation zone during ECAP. For the strain-hardening material with $m = 0.15$, the contours of effective strain reveal a dispersed zone of deformation, where elevated strain rates are noted close to the radius of the front leg and the bottom corner of the tooling. This observation implies that the primary portion of deformation transpires within these specific areas, while the flow between them maintains a relatively consistent pattern. Conversely, in the case of the strain-hardening material with $m = 0.02$, the FEM projections of effective strains and strain rates present disparities when contrasted with the situation $m = 0.15$ [112].

The contours of effective strain within the deformation zone appear to have a straighter form, implying a more even flow pattern between the radius of the front leg and the bottom corner of the tooling. This enhanced level of flow uniformity is also apparent through the narrower span and heightened consistency in the distribution of effective strain rates. Comparable trends in the forecasts of effective strain and strain rate behaviors can be seen in various material responses and tooling configurations, aligning with the grid distortion characteristics delineated earlier. These FEM results provide quantitative information about the distribution of strains and strain rates during ECAP, highlighting the interplay between material behavior, die geometry, and flow uniformity in the deformation process.

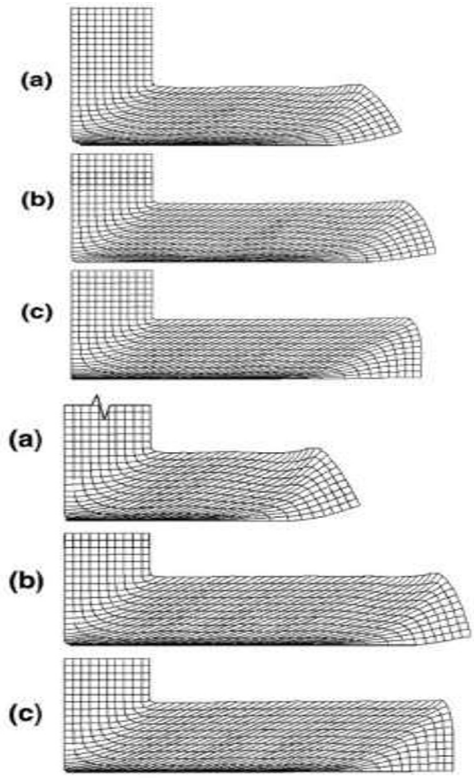

Fig. 12. Grid deformation for ECAP of a rigid perfectly plastic material for different passes [113].

The FEM predictions suggest that results in effective strain contours displayed smoother and more consistent flow patterns between the front leg radius and the bottom corner of the tooling. In the case of the strain-hardening material, regardless of whether the values of m were 0.02 or 0.15, when it underwent deformation in tooling with an mm front leg radius, nonuniformities were still evident. These results underscore the significance of considering material behavior, tooling design $R_f = 8$, and the front leg radius in influencing flow properties and the uniformity of deformation during ECAP [114]. The strain-hardening material, when combined with a sharp front leg radius, demonstrated the most advantageous conditions for attaining a high level of strain uniformity and a narrow deformation zone.

4.6 Stresses Analysis

The FEM simulations offered valuable insights into the local stresses and damage parameters during ECAP, especially in the deformation zone's centre and close to the radius of the front leg. The anticipated stress levels at the midpoint of the deformation zone, situated between the front leg corner. The bottom corner were primarily compressive in nature for all three constitutive behaviors as well as for the strain-hardening flow behavior with a value of. $m = 0.02$. This means that the stress state at the center of the deformation zone is entirely compressive, which indicates that the initiation of ductile fracture in this region is unlikely during ECAP [115]. The absence of tensile stresses suggests that the material in this region is less prone to fracture, enhancing the overall structural integrity of the billet during the ECAP process. This information can be valuable for process design and optimization, as it provides insights into the stress distribution and potential areas of vulnerability in the

material. By understanding the stress state, engineers can make informed decisions to minimize the risk of failure and enhance the overall performance of the ECAP process.

An alternative perspective on the stress state during ECAP, based on the orthogonal cutting shear plane model. On the shear plane and normal stresses might offer information. It is anticipated that a significant compressive stress will occur normal to the shear plane. Stress state is not solely shear despite the fact that the deformation in ECAP may resemble a mode of simple shear [116]. The FEM simulations also predicted a same state of stress in form compressive throughout the ECAP deformation zone, except in the vicinity of the front leg corner radius. In that specific region, it was anticipated that there would be a tensile stress component that rapidly changed with location. These findings highlight the complex stress distribution within the material during ECAP and emphasize the presence of both compressive and tensile stress components. The understanding of these stress states is crucial for assessing material behavior, predicting failure modes, and optimizing the ECAP process parameters to enhance material properties and avoid undesirable effects such as cracking or fracture [117].

4.7 Tensile Damge Parameters

In the Cockcroft and Latham model, the damage factor signifies the initiation and expansion of micro voids or cracks within the material. It operates on the premise that fracture takes place when the cumulative damage surpasses a critical threshold. The damage factor is influenced by various factors such as stress triaxiality, strain rate, and material properties.

$$C = \int (\sigma_t / \overline{\sigma}) d\overline{\varepsilon} \quad (3)$$

Within the Cockcroft and Latham model, the damage factor (C) is linked to the highest component of tensile stress σ_{max}, the effective stress σ_{eff}, and the effective strain ε_{eff}. The critical value of this damage factor (C) serves as an indicator for the point at which fracture initiation occurs [118]. In the finite element method predictions, this pertains to the behavior of a strain-hardening material with either m values of m = 0.15 or 0.02 when it undergoes deformation within a complex die with varying front leg radius (R_f) and die corner radius (R_c), Contour plots were generated to visualize the distribution of tensile damage within the material. The contour plots indicate that tensile damage tends to concentrate in specific areas within the upper regions of the extruded workpiece. The extent and magnitude of the tensile damage decrease as the value of m decreases (from 0.15 to 0.02) and as the front leg radius (R_f) increases. This implies that reducing the strain-hardening exponent (m) and increasing the front leg radius (R_f) can help mitigate tensile damage and improve the overall ductility and fracture resistance of the deformed material during ECAP. These FEM predictions provide valuable insights into the spatial distribution and severity of tensile damage, which can guide process design and parameter selection to minimize the risk of fracture and optimize the mechanical properties of the material [119]. The strain-hardening material with $m = 0.02$ mentioned the least amount of damage. In the case of complex tooling with elevated slider friction, the predictions suggested that this tooling setup was the most advantageous for diminishing tensile damage and reducing of fracture. It is likely that the back-pressure generated within such tooling plays a role in achieving this outcome. The pressing temperature was set at 1250 0C, which was chosen because at this temperature the aluminide alloy exhibits a low flow softening rate and a high strain rate sensitivity (~0.15). These characteristics help to prevent shear localization in the material. This phenomenon can be explained by the absence of tensile ductility in cast titanium aluminide under conditions of strain rates at 1 s-1 and temperatures lower than 1300 0C. The correction of the observed

crack depth using the stress contour is consistent with the expected behavior of the material in these conditions [120].

5 Conlusions

Given the susceptibility of metal flow in the ECAP process to variables like die configuration and frictional aspects, it is essential to possess a comprehensive comprehension of the precise deformation conditions within the employed die set. Such comprehension becomes pivotal when studying how strain influences the creation of ultra-fine grained materials through ECAP. Equal-Channel Angular Pressing (ECAP) has effectively decreased the grain sizes to the submicrometer range in six distinct commercially accessible AA5083 alloys. At three different material behaviours that are frequently seen in hot and cold working environments. These included behaviours that were (i) rigid and perfectly pliable; (ii) strain hardening; and (iii) flow softening. The lack of moving channel components and a "complex" layout with a sliding lower level. According to finite element modelling results, equal channel angular pressing of a strain-hardening material with low strain-rate sensitivity produced the most uniform flow. This only happened when tooling with a "front leg" radius or sharp inner corner was used. Subsequent tensile tests conducted on these alloys post-ECAP have shown a significant rise in both the 0.2% proof stress and ultimate tensile strength, even after just a single pass through the process. The 0.2% proof stress and ultimate tensile strength levels exhibited variations across different alloys, with the 5083 alloy demonstrating the highest values and the remaining alloy showing the lowest values.

References

1. Bononi, M.; Giovanardi, R. Hard anodizing of AA2011-T3 Al-Cu-Pb-Bi free-cutting alloy: Improvement of the process parameters. Corros. Sci. 2018, 141, 63–71.
2. Won, S.; Seo, B.; Park, J.M.; Kim, H.K.; Song, K.H.; Min, S.H.; Ha, T.K.; Park, K. Corrosion behaviors of friction welded dissimilar aluminum alloys. Mater. Charact. 2018, 144, 652–660.
3. Murayama, Mitsuhiro & Hono, Kazuhiro & Saga, M & Kikuchi, Masao. (1999). Atom probe studies on the early stages of precipitation in Al–Mg–Si alloys. Materials Science and Engineering: A. 250. 127-132.
4. Li, Saiyi & Beyerlein, Irene & Bourke, Mark. (2005). Texture formation during equal channel angular extrusion of fcc and bcc materials: Comparison with simple shear. Materials Science and Engineering: A. 394. 66-77.
5. Stolyarov, Vladimir & Lapovok, Rimma & Brodova, I.G. & Thomson, Peter. (2003). Ultrafine-grained Al–5 wt.% Fe alloy processed by ECAP with backpressure. Materials Science and Engineering: A. 357. 159-167.
6. Edwards, G.A. & Stiller, Krystyna & Dunlop, G. & Couper, Malcolm. (1998). The Precipitation Sequence in Al-Mg-Si Alloys. Acta Materialia. 46. 3893-3904.
7. Lapovok, Rimma. (2005). The role of back-pressure in equal channel angular extrusion. Journal of Materials Science. 40. 341-346.
8. Takeda, Mahoto & Ohkubo, F & Shirai, T & Fukui, K. (1998). Stability of metastable phases and microstructures in the ageing process of Al–Mg–Si ternary alloys. Journal of Materials Science. 33. 2385-2390.

9. Valiev, R. & Gertsman, V. & Kaibyshev, O.. (1986). Grain Boundary Structure and Properties Under External Influences. physica status solidi (a). 97. 11 - 56.
10. Höppel, Heinz & May, J. & Göken, Mathias. (2004). Enhanced Strength and Ductility in Ultrafine-Grained Aluminium Produced by Accumulative Roll Bonding. Advanced Engineering Materials. 6. 781 - 784.
11. Chuvil'deev, Vladimir. (2002). Une théorie des joints de grains hors d'équilibre et ses applications aux matériaux nano et microcristallins obtenus par extrusion dans des canaux déviés. Annales De Chimie-science Des Materiaux - ANN CHIM-SCI MAT. 27. 55-64.
12. Mckenzie, P. & Lapovok, Rimma. (2010). ECAP with back pressure for optimum strength and ductility in aluminium alloy 6016. Part 2: Mechanical properties and texture. Acta Materialia - ACTA MATER. 58. 3212-3222.
13. Hasani, Arman & Lapovok, Rimma & Tóth, László & Molinari, Alain. (2008). Deformation field variations in equal channel angular extrusion due to back pressure. Scripta Materialia - SCRIPTA MATER. 58. 771-774.
14. Hirth, S.M & Marshall, G.J & Court, Sarabjeet & Lloyd, D.J. (2001). Effect of Si on the Aging Behaviour and Formability of Alloys Based on AA6016. Materials Science and Engineering: A. s 319–321. 452–456.
15. Arzaghi, Mandana & Beausir, Benoit & Tó, L. (2009). Contribution of non-octahedral slip to texture evolution of FCC polycrystals in simple shear. Acta Materialia. 57. 2240-2453.
16. Mughrabi, Hael & Höppel, Heinz & Kautz, M. & Valiev, Ruslan. (2003). Annealing treatments to enhance thermal and mechanical stability of ultrafine-grained metals produced by severe plastic deformation. Zeitschrift für Metallkunde. 94. 1079-1083.
17. Cabibbo, M. & Evangelista, Enrico & Vedani, Maurizio. (2005). Influence of severe plastic deformations on secondary phase precipitation in a 6082 Al-Mg-Si alloy. Metallurgical and Materials Transactions A: Physical Metallurgy and Materials Science. 36. 1353-1364.
18. Tóth, L.S.. (2003). Texture Evolution in Severe Plastic Deformation by Equal Channel Angular Extrusion. Advanced Engineering Materials. 5. 308-316.
19. Li, Saiyi & Beyerlein, Irene & Alexander, David & Vogel, Sven. (2005). Texture evolution during equal channel angular extrusion: Effect of initial texture from experiment and simulation. Scripta Materialia - SCRIPTA MATER. 52. 1099-1104.
20. Hirsch, Juergen. (2009). Hot Formability and Texture Formation in Al Alloys. Materials Science Forum - MATER SCI FORUM. 604-605. 259-266.
21. Zhang, Yuhua. (2004). New approach to profile generation of disk cam mechanisms. Chinese Journal of Mechanical Engineering - CHIN J MECH ENG. 40.
22. Mckenzie, P.W.J. & Lapovok, Rimma. (2010). ECAP with back pressure for optimum strength and ductility in aluminium alloy 6016. Part 1: Microstructure. Acta Materialia - ACTA MATER. 58. 3198-3211.
23. Tsuji, Nobuhiro & Ito, Y & Saito, Y & Minamino, Yoritoshi. (2002). Strength and Ductility of Ultrafine Grained Aluminum and Iron Produced by ARB and Annealing. Scripta Materialia - SCRIPTA MATER. 47. 893-899.

24. Beyerlein, Irene & Tóth, László. (2009). Texture Evolution in Equal-Channel Angular Extrusion. Progress in Materials Science - PROG MATER SCI. 54. 427-510.
25. Zhang, Y.-S & Zhou, Y. & Jin, Q.-L. (2004). Superplasticity of Commercial 5182 and 6016 Commercial Aluminium Alloys. Transactions of Materials and Heat Treatment. 25. 35-41.
26. Fouad, D.M.; El-Garaihy,W.H.; Ahmed, M.M.Z.; El-Sayed Seleman, M.M.; Salem, H.G. Influence of multi-channel spiral twist extrusion (MCSTE) processing on structural evolution, crystallographic texture and mechanical properties of AA1100. Mater. Sci. Eng. A 2018, 737, 166–175.
27. M Saravanan, R M Pillai*, B C Pai, M Brahma kumar and K R Ravi Equal channel angular pressing of pure aluminium—an analysis‖, Bull. Mater. Sci., Vol. 29, No. 7, 679–684, (2006).
28. Hu Hong-Jun *, Zhang Ding Fei , Yang Ming Bo The die structure design of equal channel angular extrusion for AZ31 magnesium alloy based on three-dimensional finite element method, Materials and Design, 30 , pp. 2831–2840 (2009).
29. A.V.Nagasekhar, Yip Tick-Hon, H.P. Seow, Deformation behavior and strain homogeneity in equal channel angular extrusion/pressing, Journal of Materials Processing Technology, 192–193, 449–452 (2007).
30. S.C. Yoon, P. Quang, S.I. Hong, H.S. Kim Die design for homogeneous plastic deformation during equal channel angular pressing, Journal of Materials Processing Technology, 187–188, 46–50 (2007).
31. Hyoung Seop Kim, Pham Quang, Min Hong Seo, Sun Ig Hong, Kyeong Ho Baik, Hong Rho Lee and Do Minh Nghiep, “Process Modelling of Equal Channel Angular Pressing for Ultrafine Grained Materials”, Materials Transactions, Vol. 45, No. 7 , 2172 – 2176 (2004).
32. Sadasivan, N., S. Madhu, and M. Balasubramanian. "Acute angle ECAP die with modification for punchless back pressure provider." Materials Today: Proceedings 22 (2020): 1228-1232.
33. Andreyachshenko, Violetta. "Evolution of Al-Si-Mn-Fe aluminum alloy microstructure in the equal-channel angular pressing with back pressure." Materials letters 254 (2019): 433-435.
34. Comăneci, R. "Numerical analysis of back pressure equal channel angular pressing of an Al-Mg alloy." IOP Conference Series: Materials Science and Engineering. Vol. 227. No. 1. IOP Publishing, 2017.
35. Gudimetla, Kondaiah, et al. "Effect of Back Pressure on the Consolidation Behaviour of Titanium Sponge Particles Processed by ECAP." Materials Science Forum. Vol. 969. Trans Tech Publications Ltd, 2019.
36. Łyszkowski, Radosław, Wojciech Polkowski, and Tomasz Czujko. "Severe plastic deformation of Fe-22Al-5Cr alloy by cross-channel extrusion with back pressure." Materials 11.11 (2018): 2214.
37. Shen, Jianghua, et al. "Residual stress and its effect on the mechanical properties of Y-doped Mg alloy fabricated via back-pressure assisted equal channel angular pressing (ECAP-BP)." Materials Science and Engineering: A 669 (2016): 110-117.
38. Onal, E., et al. "Effect of Processing Parameters on the Magnetic Properties and Macrotexture of a Nd 13.5 Fe 73.8 Co 6.7 B 5.6 Ga 0.4 Alloy Processed by Equal

Channel Angular Pressing With Back Pressure." IEEE Transactions on Magnetics 52.7 (2016): 1-4.

39. Li, Zhuoliang, Kenong Xia, and Hua Ding. "Consolidation of pure magnesium powder by equal-channel angular pressing with back pressure." Journal of Materials Engineering and Performance 30 (2021): 2213-2219.
40. Quang, P. "The ECAP Process Simulation and Experiments with Different Back Pressures for Magnesium Alloy." Journal of Physics: Conference Series. Vol. 2219. No. 1. IOP Publishing, 2022.
41. Sankuru, Anil Babu, et al. "Effect of processing route on microstructure, mechanical and dry sliding wear behavior of commercially pure magnesium processed by ECAP with back pressure." Transactions of the Indian Institute of Metals 74 (2021): 2659-2669.
42. Jäger, A., V. Gärtnerova, and K. Tesař. "Microstructure and anisotropy of the mechanical properties in commercially pure titanium after equal channel angular pressing with back pressure at room temperature." Materials Science and Engineering: A 644 (2015): 114-120.
43. Sadasivan, N., et al. "Influence of equal channel angular pressing in an acute angle die with a back pressure notch on grain refinement, torsion and mechanical properties of aluminium." Materialwissenschaft und Werkstofftechnik 50.2 (2019): 155-164.
44. Mogucheva, A., et al. "Microstructural evolution in a 5024 aluminum alloy processed by ECAP with and without back pressure." Materials Science and Engineering: A 560 (2013): 178-192.
45. K. Kowalczyk, M.B. Jabłońska, M. Tkocz, R. Chulist, I. Bednarczyk, T. Rzychoń, Effect of the number of passes on grain refinement, texture and properties of DC01 steel strip processed by the novel hybrid SPD method, Archives of Civil and Mechanical Engineering 22 (2022) 115. https://doi.org/10.1007/s43452-022-00432-6.
46. X. Wang, Z. Xiao, X.P. Meng, Y.H. Yi, L. Chen, Microstructure and properties evolution of Cu-Ti-Cr-Mg alloy during equal channel angular pressing at room temperature and cryogenic temperature, J. Alloys Compd. 927 (2022) 166940. https://doi.org/10.1016/j.jallcom.2022.166940.
47. F. Caldatto Dalan, G.F. de Lima Andreani, D.N. Travessa, I.A. Faizov, S. Faizova, K.R. Cardoso, Effect of ECAP processing on distribution of second phase particles, hardness and electrical conductivity of Cu-0.81Cr−0.07Zr alloy, Transactions of Nonferrous Metals Society of China 32 (2022) 217-232. https://doi.org/10.1016/S1003-6326(21)65789-8.
48. H.S. Kim, Y.Kim, K.H.Song, Effect of post-heat-treatment in ECAP processed Cu-40%Zn brass. Journal of Alloys and Compounds 536 (2012) 200-203. https://doi.org/10.1016/j.jallcom.2011.11.079.
49. H. R. Naser, M. M. Talib, AMH Aljassani, Influence of ECAP processing on mechanical and wear properties of brass alloy. Materials Today: Proceedings 44 (2021) 2399–2402. https://doi.org/10.1016/j.matpr.2020.12.461.
50. M. Demirtas, Microstructural, mechanical and tribological characterization of Cu-CoNi-Be alloy processed via equal channel angular pressing. Materials Today Communications 28 (2021) 102676 https://doi.org/10.1016/j.mtcomm.2021.102676.

51. E. Cagatay, Effect of severe plastic deformation on the precipitation kinetics and the properties of CuCoNiBe alloys. Materials Today Communications 31 (2022) 103473 https://doi.org/10.1016/j.mtcomm.2022.103473.
52. V.U. Kazykhanov, M.Y. Murashkin, Influence of deformation at elevated temperatures on stability of microstructure and mechanical properties of UFG aluminum alloy, Materials Letters 301 (2021) 130328. https://doi.org/10.1016/j.matlet.2021.130328.
53. C. Wang, A. Ma, J. Jiang, Effect of ECAP process on as-cast and as-homogenized MgAl-Ca-Mn alloys with different Mg2Ca morphologies, Journal of Alloys and Compounds 793 (2019) 259-270. https://doi.org/10.1016/j.jallcom.2019.04.202.
54. M. Ma et al. Development of homogeneity in a Cu-Mg-Ca alloy processed by equal channel angular pressing, Journal of Alloys and Compounds 11 (2019) 153112. https://doi.org/10.1016/j.jallcom.2019.153112.
55. K. Abib et al, On the microstructure and texture of Cu-Cr-Zr alloy after severe plastic deformation by ECAP, Materials Characterization 112 (2016) 252-258. http://dx.doi.org/10.1016/j.matchar.2015.12.026.
56. M. Muzhi, Z. Li, W. Qiu et al. Microstructure and properties of Cu–Mg-Ca alloy processed by equal channel angular pressing, Journal of Alloys and Compounds, 788 (2019) 50-60. https://doi.org/10.1016/j.jallcom.2019.01.335.
57. J. Bursik, V. Bursikova, M. Svoboda, P. Kral, J. Dvorak, V. Sklenicka, Microstructure and local mechanical properties of Cu-Co alloys after severe plastic deformation, Key Engineering Materials 586 (2013) 100-103. https://doi.org/10.4028/www.scientific.net/KEM.586.100.
58. A. Bachmaier, J. Schmauch, H. Aboulfadl, A. Verch, C. Motz, On the process of codeformation and phase dissolution in a hard-soft immiscible CuCo alloy system during high-pressure torsion deformation, Acta Materialia 115 (2016) 333-346. https://doi.org/10.1016/j.actamat.2016.06.010.
59. A. Bachmaier, H. Aboulfadl, M. Pfaff, F. Mücklich, C. Motz, Structural evolution and strain induced mixing in Cu–Co composites studied by transmission electron microscopy and atom probe tomography, Materials Characterization 100 (2015) 178-191. https://doi.org/10.1016/j.matchar.2014.12.022.
60. K. Bartha, A. Veverková, J. Stráský, J. Veselý, M. Janeček, Effect of the severe plastic deformation by ECAP on microstructure and phase transformations in Ti-15Mo alloy Materials Today Communications 22 (2020) 100811. https://doi:10.1016/j.mtcomm.2019.10081121.
61. N.S.D. Vincentis, A. Kliauga, M. Ferrante, M Avalos, H.G. Brokmeier, R.E. Bolmaro, Evaluation of microstructure anisotropy on room and medium temperature ECAP deformed F138 steel, Materials Characterization 107 (2015) 98-111. https://doi.org/10.1016/j.matchar.2015.06.035.